Higgs boson mass predictions in supergravity unification, recent LHC-7 results, and dark matter

Sujeet Akula,[1] Baris Altunkaynak,[1] Daniel Feldman,[2] Pran Nath,[1] and Gregory Peim[1]

[1]*Department of Physics, Northeastern University, Boston, Massachusetts 02115, USA*
[2]*Department of Physics, University of Michigan, Ann Arbor, Michigan, USA*
(Received 21 December 2011; published 2 April 2012)

LHC-7 has narrowed down the mass range of the light Higgs boson. This result is consistent with the supergravity unification framework, and the current Higgs boson mass window implies a rather significant loop correction to the tree value, pointing to a relatively heavy scalar sparticle spectrum with universal boundary conditions. It is shown that the largest value of the Higgs boson mass is obtained on the hyperbolic branch of radiative breaking. The implications of light Higgs boson in the broader mass range of 115 GeV to 131 GeV and a narrower range of 123 GeV to 127 GeV are explored in the context of the discovery of supersymmetry at LHC-7 and for the observation of dark matter in direct detection experiments.

I. INTRODUCTION

In models based on supersymmetry, the light Higgs boson [1] has a predictive mass range, and recently LHC-7 has stringently constrained the light Higgs boson to lie in the 115 GeV to 131 GeV range (ATLAS) and the 115 GeV to 127 GeV range (CMS) at the 95% confidence level [2] with possible hints of evidence within a few GeV of 125 GeV. This mass window lies in the range predicted by supergravity unification (SUGRA) [3] (for reviews see [4–6]). In this work we investigate supergravity model points that are consistent with the mass range given by the new LHC-7 data [2] (for a previous work on the analysis of the Higgs boson in SUGRA and string models pointing to a heavier Higgs in the 120 GeV range see [7]).

LHC-7 has made great strides in exploring the parameter space of supersymmetric models. Indeed, early theoretical projections for the expected reach in sparticle masses and in the $m_0 - m_{1/2}$ plane for LHC-7 [8–11] have been met and exceeded by the 1 fb^{-1} and 2 fb^{-1} LHC-7 data [12–16]. The implications of the new LHC results have been analyzed by a number of authors in the context of lower limits on supersymmetric particles and in connection with dark matter [17–23]. Now the most recent results from CERN [2] indicate that the two detectors, ATLAS and CMS, have collected as much as 5 fb^{-1} of data. One of the most interesting implications of the LHC-7 data concerns the constraints it imposes on the Higgs boson mass.

As mentioned above, we will work within the framework of a supergravity grand unification model with universal boundary conditions [3,24,25]. Here we discuss the dependence of the light Higgs boson mass on the parameter space, i.e., on m_0, $m_{1/2}$, A_0, $\tan\beta$ [26], where m_0, $m_{1/2}$ and A_0 are the parameters at the GUT scale, where the GUT scale, $M_{\rm GUT} \sim 2 \times 10^{16}$ GeV is defined as the scale at which the gauge couplings unify, and where m_0 is soft scalar mass, $m_{1/2}$ is the gaugino mass, A_0 is the trilinear

coupling and $\tan\beta$ is the ratio of the two Higgs VEVs in the minimal supersymmetric standard model.

An important aspect of SUGRA models is that the radiative electroweak symmetry breaking (REWSB) is satisfied for A_0/m_0 typically in the -5 to 5 range. The renormalization group evolution then leads to a value of the trilinear coupling, A_t, at the electroweak scale to also be $\mathcal{O}({\rm TeV})$. The relevance of this observation is that, quite generically, supergravity unification leads to a sizable A_t which is needed to give a substantial leading-order loop correction to the Higgs boson mass for any fixed μ, $\tan\beta$, and m_0, where μ is the Higgs mixing parameter in the superpotential. Thus a generic prediction of SUGRA models under radiative electroweak symmetry breaking for a sizable A_0/m_0 is that there would be a substantial loop correction to the Higgs boson mass, and it is well known that the light Higgs mass at the tree level has the value $m_{h^0} \leq M_Z$ and there is a significant loop correction Δm_{h^0} to lift it above M_Z [27–33].

The dominant one-loop contribution arises from the top/stop sector and is given by

$$\Delta m_{h^0}^2 \simeq \frac{3m_t^4}{2\pi^2 v^2} \ln\frac{M_{\rm S}^2}{m_t^2} + \frac{3m_t^4}{2\pi^2 v^2}\left(\frac{X_t^2}{M_{\rm S}^2} - \frac{X_t^4}{12M_{\rm S}^4}\right), \quad (1)$$

where $v = 246$ GeV, $M_{\rm S}$ is an average stop mass, and X_t is given by

$$X_t \equiv A_t - \mu\cot\beta. \quad (2)$$

From Eq. (1) one finds that the loop correction is maximized when

$$X_t \sim \sqrt{6}M_{\rm S}. \quad (3)$$

We note that there can be important loop corrections also from the b-quark sector and a correction similar to Eq. (1) can be written where X_t is replaced by $X_b = A_b - \mu\tan\beta$ along with other appropriate replacements. Thus, when $\mu\tan\beta$ becomes large, the b-quark contribution to the

loop correction, which is proportional to powers of X_b, becomes large and is comparable to the top contribution, which implies that a high Higgs mass can also result in stau-coannihilation models where typically $m_{1/2}$ is large and m_0 is relatively small.

Further, we note that the approximation of Eq. (3) would not hold if the off-diagonal elements of the stop mass squared matrix are comparable to the diagonal elements which can happen for very large A_t. In addition, it is well-known that the two-loop corrections are substantial (see, e.g., [34] for a numerical analysis). While the correction at the one-loop level has the symmetry $X_t \rightarrow -X_t$, this symmetry is lost when the two-loop corrections are included and then (A_0/m_0) plays an important role in the corrections to the Higgs boson mass. As seen later, this observation is supported by the full numerical analysis which includes the two-loop corrections. We note in passing that the theoretical predictions for the light Higgs boson mass depend sensitively on the input parameters which include the gauge coupling constants as well as the top mass with their experimental errors. Additionally, there are also inherent theoretical uncertainties, which, together with the uncertainties of the input parameters, allow theoretical predictions of the light Higgs boson mass to be accurate to only within an error corridor of a few GeV (see, e.g., [34]).

Since the loop corrections involve the sparticle spectrum, a large loop correction implies a relatively heavy sparticle spectrum and specifically heavy scalars. Such a possibility arises in REWSB, which allows for scalars heavier than 10 TeV [35]. Specifically, with scalars approaching 10 TeV, the Higgs boson mass can remain heavy while the gaugino sector is free to vary. This occurs within the minimal SUGRA framework and similar situations arise in other works of radiative breaking [36,37].

Indeed, quite generally in SUGRA and string models with the MSSM field content, the analysis of the Higgs mass with loop corrections under the constraints of REWSB gives an upper limit on the light Higgs boson mass of about 135 GeV for a wide range of input parameters.[1] A very interesting aspect of the recent LHC-7 data concerns the fact that a large portion of the Higgs boson mass window has been excluded and what remains is consistent with the range predicted by the SUGRA models.

II. HIGGS MASS IN MINIMAL SUGRA

We discuss now the dependence of the light Higgs boson mass on the SUGRA parameter space. The numerical analysis was done using a uniformly distributed random scan over the soft parameters with sign $(\mu) = 1$, $m_{1/2} < 5$ TeV, $|A_0/m_0| \leq -8$, $\tan\beta \in (1, 60)$ and two different

---

[1]We note that heavier Higgs boson masses can be obtained in a variety of different models, such as hierarchical breaking models [38–40] (for recent work see [41,42]) or by addition of vector like multiplets [43].

ranges for m_0. One scan was done sampling over lower values of m_0, i.e., $m_0 \leq 4$ TeV, and has roughly 10×10^6 mSUGRA model points (where a model point is defined as one set of the mSUGRA input parameters). The other scan was done sampling over larger values of m_0, i.e., $m_0 \gtrsim 4$ TeV, and contains approximately 24×10^6 mSUGRA model points. For the scan sampling over large values of m_0, we have imposed the upper bound of $m_0 = 100$ TeV.

Experimental constraints were then applied to these mSUGRA model points, which include the limits on sparticle masses from LEP [44]: $m_{\tilde{\tau}_1} > 81.9$ GeV, $m_{\tilde{\chi}_1^\pm} > 103.5$ GeV, $m_{\tilde{t}_1} > 95.7$ GeV, $m_{\tilde{b}_1} > 89$ GeV, $m_{\tilde{e}_R} > 107$ GeV, $m_{\tilde{\mu}_R} > 94$ GeV, and $m_{\tilde{g}} > 308$ GeV. Additionally, we apply the WMAP [45] 4σ upper bound, i.e., $\Omega_\chi h^2 < 0.1344$. We define $(\Omega_\chi h^2)_{\text{WMAP}} \equiv 0.1120$, the central value from the WMAP-7 data. Only taking the WMAP upper limit allows for the possibility of multi-component dark matter [46]. Other constraints applied to the mSUGRA parameter points include the $g_\mu - 2$ [47] constraint $(-11.4 \times 10^{-10}) \leq \delta(g_\mu - 2) \leq (9.4 \times 10^{-9})$ and constraints from B-physics measurements [48–50], which yield flavor constraints from the data, i.e., $(2.77 \times 10^{-4}) \leq \mathcal{B}r(b \rightarrow s\gamma) \leq (4.37 \times 10^{-4})$ (where this branching ratio has the NNLO correction [51]) and $\mathcal{B}r(B_s \rightarrow \mu^+\mu^-) \leq 1.1 \times 10^{-8}$. As done in [20,52], we will refer to these constraints as the *general constraints*. These constraints were imposed using MICROMEGAS [53] for the relic density as well as for the indirect constraints and SOFTSUSY [54] for the sparticle mass spectrum. The model points are generated with SOFTSUSY version 3.2.4 which includes an important bug fix for heavy scalars when computing m_{h^0}.

We display the model points consistent with the general constraints in Fig. 1 and in Fig. 2. In the left panel of Fig. 1 we exhibit the Higgs boson mass as a function of m_0 for the case when $\tan\beta > 20$, and in the right panel we exhibit it for the case when $\tan\beta < 20$. In both cases we see a slow logarithmic rise of m_{h^0} with m_0 for large m_0. In the left and middle panels of Fig. 2 we show the distribution of the light Higgs boson mass in the $\tan\beta - A_0/m_0$ plane. One finds that a large part of the parameter space exists where the Higgs boson mass lies in the range $m_{h^0} > 115$ GeV (left panel) or in the narrower range $m_{h^0} > 123$ GeV (middle panel). In the right panel of Fig. 2, we show the distribution of $\log(m_0)$ (where m_0 is in GeV units) in the $m_{h^0} - A_0/m_0$ plane.

Our analysis shows a range of possibilities where a heavier Higgs boson, i.e., $m_{h^0} \gtrsim 125$ GeV, can arise in the minimal supergravity model. Thus, for values of $m_0 < 4$ TeV, a heavier Higgs boson mass can be gotten for a large A_0/m_0 (typically of size ± 2 with a significant spread). In Fig. 3 we give an illustration of the cancellation in REWSB to produce μ where we plot μ vs $|m_{H_2}(Q)|$ for different regions of the parameter space. Regions with small μ and large $|m_{H_2}(Q)|$ imply a large cancellation in
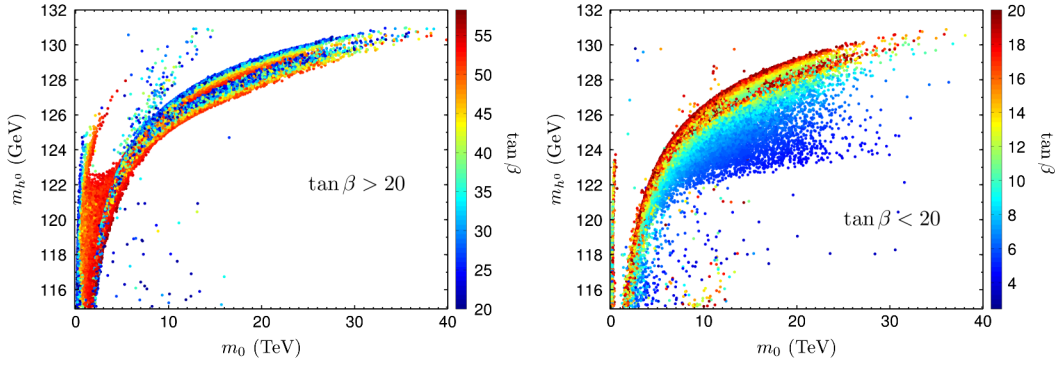
FIG. 1 (color online).   Left: Exhibition of the light Higgs mass as a function of m_0 for $\tan\beta > 20$. Right: Same as the left panel except that $\tan\beta < 20$. The data analyzed passes the general constraints and are generated with both scans of m_0.
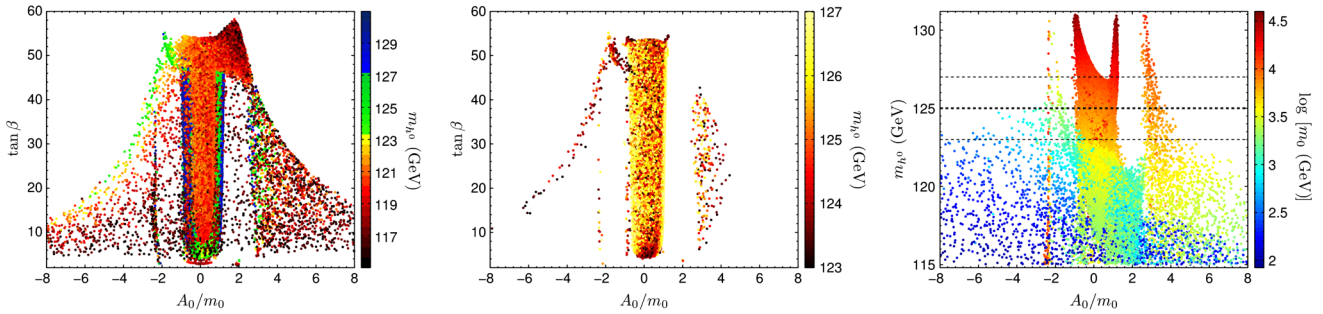

FIG. 2 (color online).   Left: A display of the model points in the $\tan\beta - A_0/m_0$ plane when $m_{h^0} > 115$ GeV. Model points are shaded according to their light Higgs boson mass, m_{h^0}. Middle: Same as the left panel except that $m_{h^0} > 123$ GeV. Right: Exhibition of the model points in the $m_{h^0} - A_0/m_0$ plane displayed by $\log(m_0)$ with m_0 in GeV units. It is seen that for low values of $|A_0/m_0|$ larger m_0 corresponds to a heavier light Higgs boson. The data analyzed passes the *general constraints* and are generated with both scans of m_0 as discussed in the text.
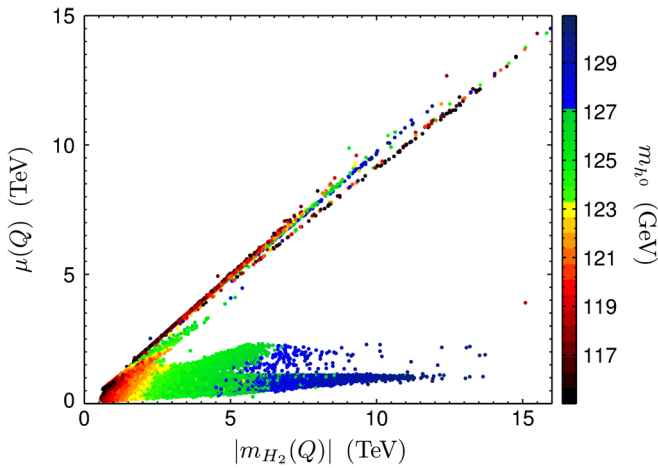

FIG. 3 (color online).   An exhibition of μ vs $|m_{H_2}(Q)|$ as an illustration of the degree of cancellation in different regions of the parameter space. One finds that, on the upper branch, μ is comparable to $|m_{H_2}(Q)|$, showing that there is not much cancellation in REWSB to produce μ. On the lower branch one finds that $|m_{H_2}(Q)|$ can get large while μ remains small pointing to significant cancellations in REWSB.

REWSB, as in the lower branch of Fig. 3, while regions with a μ comparable to $|m_{H_2}(Q)|$ imply a small cancellation. We note, however, that even a large cancellation occurs quite naturally because of the structure of the REWSB. For values of $m_0 > 4$ TeV, a heavier Higgs boson mass for relatively smaller values of A_0/m_0 is also allowed. For this case, the first- and second-generation sfermions may be difficult to observe while the third-generation sfermions would still be accessible. However, for the first case, where a Higgs mass $m_{h^0} \gtrsim 125$ GeV arises for low m_0 and relatively larger $|A_0/m_0|$, the observation of signals arising from the production of first- and second-generation sfermions and heavier SUSY Higgses remains very much within reach of the LHC with sparticles of relatively low mass in the spectrum, and variable mass hierarchies present [55]. This will be shown in more detail in the next section.

III. SPARTICLE SPECTRA AND HIGGS MASS

There are some interesting correlations between the light Higgs and the sparticle spectrum. As noted already, a larger light Higgs boson mass typically indicates a

relatively heavier sparticle spectrum. We give now a more quantitative discussion using the two scans discussed in the previous section after imposing the general constraints. In Table I we present the lower limits on some of the sparticles as the light Higgs mass gets progressively larger between $m_{h^0} = 115$ GeV and $m_{h^0} = 127$ GeV, showing the results of the two scans (upper and lower tables). The top panel of the table is for the low value sampling of m_0, i.e., the scan with $m_0 \leq 4$ TeV, and the middle panel is for the large value sampling of m_0, i.e., the scan with m_0 between 4 TeV and 100 TeV. In the bottom panel, we give benchmark points with the sparticle masses near the lower limits presented. Thus, after applying an additional 800 GeV gluino cut on the models, for the low m_0 scan we find that a light Higgs boson mass of $m_{h^0} = 115$ GeV allows for a lightest neutralino mass of around 80 GeV, but $m_{h^0} = 125$ GeV

indicates a lightest neutralino mass of around 220 GeV. The value of 220 GeV is consistent with independent constraints coming from the search for squarks and gluinos at the LHC (see [19,20]). For the cases $m_{h^0} = 115$ GeV and $m_{h^0} = 125$ GeV corresponding masses for the lightest chargino, $\tilde{\chi}_1^\pm$, (degenerate with the second lightest neutralino, $\tilde{\chi}_2^0$) are 100 GeV and 425 GeV; for the gluino, $\tilde{g}$, 800 GeV and 1.3 TeV; for the first- and second-generation squarks, $\tilde{q}$, 730 GeV and 2.2 TeV, and for the first- and second-generation sleptons, $\tilde{\ell}$, 150 GeV and 1.6 TeV. Thus, for the low m_0 scan, the shifts in lower limits are dramatic for the gluino and for the first-generation sfermions. The stop, $\tilde{t}_1$, and the stau, $\tilde{\tau}_1$, however, continue to be relatively light. The $\tilde{\tau}_1$ mass, though, is very sensitive to the higher mass bins in the light Higgs mass, i.e., bins greater then 123 GeV.

TABLE I. Display of the lower limits on the sparticle masses as a function of a lower bound on the light Higgs mass for the mSUGRA models. The top panel shows the sparticle lower bounds for the small m_0 scan and the middle panel shows the sparticle lower bounds for the large m_0 sampling. The model points in both cases pass the *general constraints* as well as an additional constraint that the gluino mass exceed 800 GeV. We note that the lower bound limits for the sparticles are not necessarily for the same model point. All masses are in GeV. A remarkable aspect of the analysis is that a stop mass as low as 300 GeV can be obtained for parameter points with $m_0 > 4$ TeV. We further note that in this region one has the possibility of the first two neutralinos and the light chargino being degenerate as seen above when μ is smaller than the electroweak gaugino masses $\tilde{m}_1$ and $\tilde{m}_2$. In the bottom panel, we give benchmark points that show the regions of parameter space that give masses near the minima presented, which shows how some but not all of the lower limits may be obtained by specific points.

	$m_{h^0} > 115$	$m_{h^0} > 117$	$m_{h^0} > 119$	$m_{h^0} > 121$	$m_{h^0} > 123$	$m_{h^0} > 125$	$m_{h^0} > 127$
$m_{H^0} \sim m_{A^0}$	212	216	273	324	1272	1517	2730
$m_{H^\pm}$	230	234	288	337	1275	1520	2732
$m_{\tilde{\chi}_1^0}$	81	81	81	88	193	218	236
$m_{\tilde{\chi}_1^\pm} \sim m_{\tilde{\chi}_2^0}$	104	104	104	111	376	424	459
$m_{\tilde{g}}$	800	800	803	803	1133	1264	1373
$m_{\tilde{t}_1}$	156	197	228	230	231	246	260
$m_{\tilde{\tau}_1}$	142	161	201	232	321	576	1364
$m_{\tilde{q}}$	729	796	995	1126	1528	2235	2793
$m_{\tilde{\ell}}$	163	194	265	325	475	1631	2557
μ	107	107	107	120	1418	1863	2293

	$m_{h^0} > 115$	$m_{h^0} > 117$	$m_{h^0} > 119$	$m_{h^0} > 121$	$m_{h^0} > 123$	$m_{h^0} > 125$	$m_{h^0} > 127$
$m_{H^0} \sim m_{A^0}$	287	287	287	338	367	548	644
$m_{H^\pm}$	301	301	301	349	378	555	646
$m_{\tilde{\chi}_1^0}$	91	91	91	91	91	91	256
$m_{\tilde{\chi}_1^\pm} \sim m_{\tilde{\chi}_2^0}$	104	104	104	104	104	104	264
$m_{\tilde{g}}$	802	802	802	802	925	1006	1813
$m_{\tilde{t}_1}$	229	229	229	229	229	360	360
$m_{\tilde{\tau}_1}$	911	911	911	911	1186	1186	1186
$m_{\tilde{q}}$	4035	4035	4035	4035	4215	4493	4493
$m_{\tilde{\ell}}$	3998	3998	3998	4002	4085	4308	4308
μ	118	118	118	118	138	140	251

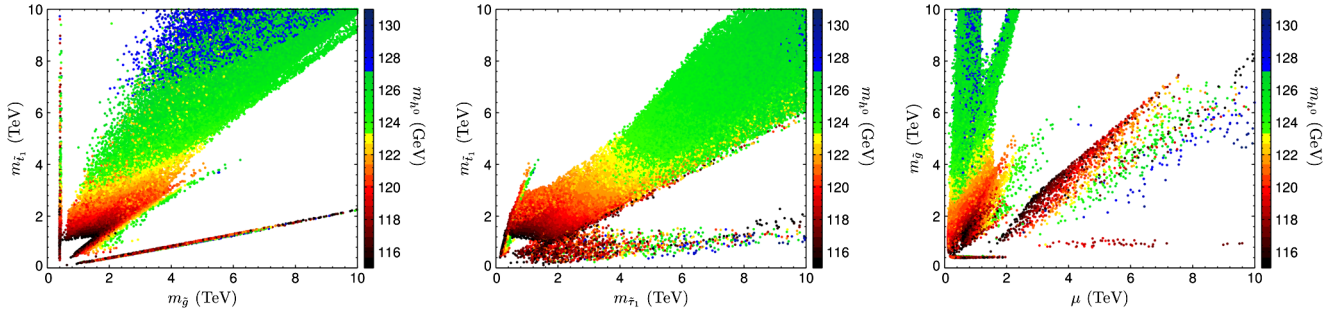| Benchmark	m_0	$m_{1/2}$	A_0/m_0	$\tan\beta$	m_{h^0}	$m_{\tilde{\chi}_1^0}$	$m_{\tilde{\chi}_1^\pm}$	$m_{\tilde{g}}$	$m_{\tilde{t}_1}$	$m_{\tilde{\tau}_1}$	$m_{\tilde{q}}$	$m_{\tilde{\ell}}$	μ
Light stop	5108	764	2.549	33.29	125	321	621	1828	334	3604	5240	5108	3887
Light gauginos, low μ	3340	306	−0.395	29.521	121	91	115	832	1974	3070	3352	3335	125
Light stau	248	548	−6.834	14	121	228	438	1254	569	232	1126	325	1072

FIG. 4 (color online).   Analysis is based on the general constraints discussed in the text and for both scans of m_0. Left panel: Exhibition of the stop vs the gluino mass in the mass window where both the stop and the gluino masses run till 10 TeV. Middle panel: Exhibition of stop mass vs stau mass. Right panel: Exhibition of the gluino mass vs μ.

For the large m_0 scan, the sparticle lower limits are modified in a significant way. Most noticeably, the electroweak gaugino spectrum can remain light at higher Higgs mass relative to what one finds in the more restrictive low m_0 scan. Further, we observe that as the Higgs mass grows, the value of μ can remain a few times the Z mass, whereas in the low m_0 scan this does not occur. In addition, we can see that the sfermion bounds do not change as drastically as the Higgs mass changes as they did with the low m_0 scan, and, in particular, the masses of the other Higgses A^0, H^0, $H^\pm$ can remain much lighter.

More graphically, in Fig. 4 we compare ranges on the sparticle masses distributed by a light Higgs mass. Thus the left panel of Fig. 4 gives a plot of the stop mass vs the gluino mass and the middle panel gives a plot of the stop mass vs the stau mass. These correlations of the light Higgs mass with the respective sparticle masses show directly how a determination of the Higgs mass at the LHC will constrain the masses of the R-parity odd particles. The right panel of Fig. 4 gives a display of the gluino mass vs μ (the Higgsino mass parameter at the scale Q where electroweak symmetry breaking occurs). Here one finds that a μ, as small as a 200 GeV, can generate a Higgs boson mass up to about 122 GeV. However, the larger Higgs masses, i.e., Higgs masses above 125 GeV, can also have μ of size that is sub-TeV. Thus, one can have a

heavier Higgs, scalars in the several TeV region, but still have a light μ [7,35,36].

IV. HYPERBOLIC BRANCH OF REWSB AND FOCAL SURFACES

It is known that the radiative electroweak symmetry breaking carries in it a significant amount of information regarding the parameter space of SUGRA models. Thus REWSB allows for a determination of μ^2 in terms of the soft parameters [35,56] (for further works see [57]) so that the breaking of electroweak symmetry is encoded in the following expression

$$\mu^2 = -\frac{1}{2}M_Z^2 + m_0^2 C_1 + A_0^2 C_2 + m_{1/2}^2 C_3 + m_{1/2}A_0 C_4 + \Delta\mu_{\text{loop}}^2, \tag{4}$$

where C_i, i running from 1 to 4, depend on the top mass, $\tan\beta$ and Q. It was shown in [35] that one can classify regions of Eq. (4) in the following two broad classes: the ellipsoidal branch, denoted EB, where $C_1 > 0$, and the hyperbolic branch, denoted HB, where $C_1 \leq 0$. More recently in [52] it was shown that HB can be further classified into three regions. One such region was defined as the focal point, HB/FP, where $C_1 = 0$. It was further shown that the HB/FP limits to the focus point [58] when $\tan\beta \gg 1$.
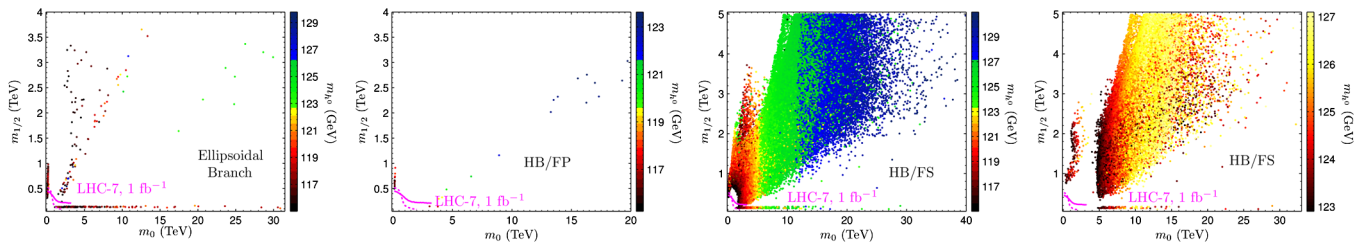

FIG. 5 (color online).   Analysis of the Higgs boson mass in Focal Regions. The analysis is done for the model points that satisfy the low m_0 sampling and the general constraints. Left: Shows the EB region with the light Higgs boson mass greater than 115 GeV. We see that the majority of these points are not in the heavy Higgs boson region. Middle Left: Displays the HB/FP where we see that there are no Higgs masses greater then 120 GeV. In the right two panels we display the HB/FS (which include HB/FC) as follows: in the middle right panel we exhibit the HB/FS model points for the Higgs mass range above 115 GeV and in the right panel we exhibit the HB/FS model points that have the light Higgs boson mass between 123 GeV and 127 GeV. In all panels the dotted magenta line corresponds to the curve CMS given in Ref. 2 of [12] and the solid magenta line corresponds to the ATLAS curve of Ref. 1 of [16].

Another region defined was the focal curve, HB/FC, where $C_1 < 0$ and two soft parameters are free to get large, i.e., either m_0, A_0 or m_0, $m_{1/2}$. The last region was defined to be the focal surface, HB/FS, where $C_1 < 0$ and three soft parameters were free to get large, i.e., m_0, A_0, $m_{1/2}$. It was further shown in [52] that HB/FC was a subset of HB/FS and that the HB/FP was mostly depleted after imposing constraints from flavor physics, WMAP, sparticle mass lower limits, and LHC-7. However, other regions of the parameter space were found to be well populated.

In Fig. 5 we give an analysis of the Higgs mass ranges lying on the EB and on the focal regions with a comparison to the LHC-7 curves (Ref. 1 of [16] and Ref. 2 of [12]). In the top two panels we consider the Higgs mass range upwards of 115 GeV. The left panel is for the ellipsoidal branch and the middle left panel is for the focal point region. In the EB region, one finds that the majority of light Higgs boson masses do not exceed 124 GeV, while in the HB/FP region the Higgs masses do not get beyond 120 GeV except perhaps for some isolated points. Further, the HB/FP region is highly depleted as can be seen by the paucity of allowed model points in the middle left panel of Fig. 5. The largest Higgs boson masses are achieved on HB/FS, which includes HB/FC, shown in the right two panels of Fig. 5, where the region above a Higgs boson mass of 115 GeV (middle right) and between 123 GeV and 127 GeV (right) are shown. The right panel shows that the Higgs mass region within a few 125 GeV is well populated.

V. HIGGS BOSON AND DARK MATTER

There is a strong correlation between the light Higgs mass and dark matter. It has already been pointed out that annihilation via the Higgs pole can generate the relic density to be consistent with WMAP (see the first paper of [17]). In this case the neutralino mass would be roughly half the light Higgs boson mass. For heavier neutralino masses other annihilation mechanisms become available. We would be interested in the cases which include large m_0 and specifically in the spin-independent proton-neutralino cross section in this domain. For this case when m_0 is large the s-channel squark exchange which contributes to the spin-independent proton-neutralino cross section becomes suppressed while the t-channel Higgs exchange dominates. The scattering cross section in this case is given by

$$\sigma^{\mathrm{SI}}_{\tilde{\chi}^0_1 N} = (4\mu^2_{\tilde{\chi}^0_1 N}/\pi)(Z f_p + (A - Z) f_n)^2. \qquad (5)$$

Here $f_{p/n} = \sum_{q=u,d,s} f^{(p/n)}_{T_q} C_q \frac{m_{p/n}}{m_q} + \frac{2}{27} f^{(p/n)}_{TG} \sum_{q=c,b,t} \times C_q \frac{m_{p/n}}{m_q}$, where the form factors $f^{(p/n)}_{T_q}$ and $f^{(p/n)}_{TG}$ are given in [53,59,60] and the couplings C_q are given by [59,60]

$$C_q = -\frac{g_2 m_q}{4 m_W \delta_3}\left[(g_2 n_{12} - g_Y n_{11})\delta_1 \delta_4 \delta_5\left(-\frac{1}{m^2_H} + \frac{1}{m^2_h}\right) \right.$$
$$\left. + (g_2 n_{12} - g_Y n_{11})\delta_2\left(\frac{\delta^2_4}{m^2_H} + \frac{\delta^2_5}{m^2_h}\right)\right]. \qquad (6)$$

For up quarks one has $\delta_i = (n_{13}, n_{14}, s_\beta, s_\alpha, c_\alpha)$ and for down quarks $\delta_i = (n_{14}, -n_{13}, c_\beta, c_\alpha, -s_\alpha)$, where i runs from 1 to 5, α is the neutral Higgs mixing parameter, n_{1j} is the neutralino eigencontent, c_α denotes $\cos\alpha$ and s_α denotes $\sin\alpha$. The above approximation holds over a significant part of the parameter space specifically for large m_0 and we have checked that it compares well with the full analysis where the full theory calculation is done with MICROMEGAS. In the analysis work presented here, however, we exhibit only the results of the full analysis. In Fig. 6 we give a plot of the proton-neutralino
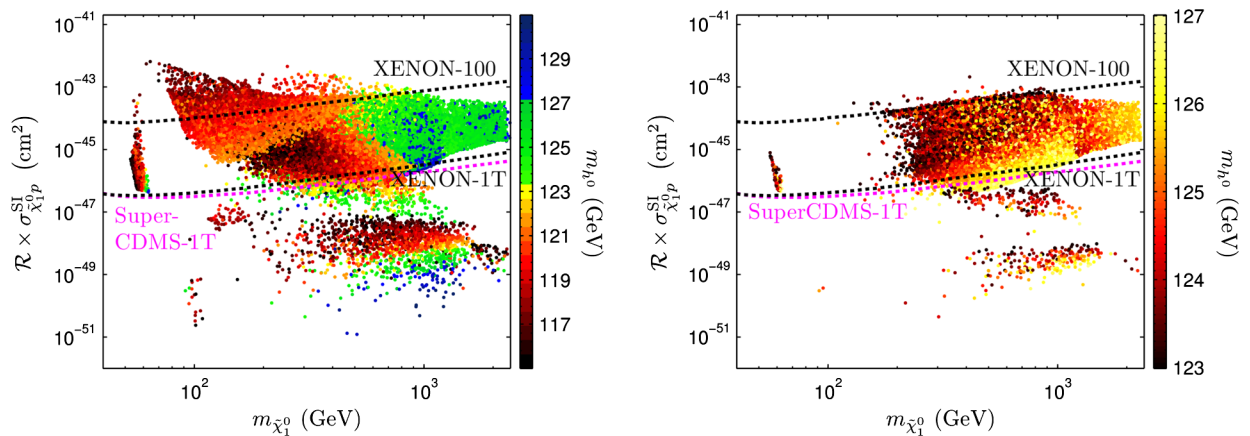

FIG. 6 (color online). Exhibition of proton-neutralino spin-independent cross section against the neutralino mass. Here we see that models with a Higgs boson mass in the range consistent with the results from LHC-7 will be probed in the next round of dark matter experiments. In the plots the proton-neutralino spin-independent cross section was corrected by $\mathcal{R} \equiv (\Omega h^2)/(\Omega h^2)_{\mathrm{WMAP}}$ to allow for multicomponent dark matter. The analysis is done for the model points passing the general constraints from the low m_0 sampling. The left panel gives the full light Higgs boson mass range, i.e., 115 GeV to 131 GeV and the right panel only deals with the sensitive region between 123 GeV to 127 GeV.

spin-independent cross section, $\sigma^{\mathrm{SI}}_{\tilde{\chi}^0_1 p}$ times $\mathcal{R}$ plotted as a function of the neutralino mass where we have corrected $\sigma^{\mathrm{SI}}_{\tilde{\chi}^0_1 p}$ by a factor $\mathcal{R} \equiv (\Omega h^2)/(\Omega h^2)_{\mathrm{WMAP}}$ to take into account the possibility of multicomponent dark matter. The points are shaded according to the Higgs boson masses and we show the XENON-100 [61] exclusion curve as well as the XENON-1T [62] and the SuperCDMS [63] projections.

It is important to observe that when the Higgs mass region 123 GeV to 127 GeV is considered, nearly all of the mSUGRA parameter points that lie in this region which are also consistent with the general constraints (from our low m_0 and high m_0 scans) give rise to neutralino mass and proton-neutralino spin-independent cross section (scaled by $\mathcal{R}$), that lies just beyond what the most recent results from the XENON collaboration have probed. However, a vast majority of this region is projected to be explored by XENON-1T and SuperCDMS. This point is clearly seen in the right panel of Fig. 6.

VI. CONCLUSION

Recent data from LHC-7 indicates a narrow window on the light Higgs mass. This allowed mass window is consistent with the range predicted by SUGRA models and specifically by the mSUGRA model. Here we discussed the implications of the indicated mass range for the light Higgs mass for the sparticle mass spectrum and for dark matter. Using the allowed Higgs mass range above 115 GeV, the corresponding ranges for the soft masses and couplings, as well as the ratio of the vacuum expectation values of the Higgs doublets and the Higgsino mass parameter, were found. We then investigated the ranges for the sparticle masses correlated to the predicted value of the Higgs boson mass, specifically for the chargino, the neutralino, the gluino, the stop, the stau, for the first- and

second-generation squarks and sleptons and for the heavier Higgs of the minimal supersymmetric standard model, i.e., the *CP* odd Higgs A^0, the *CP* even Higgs H^0, and the charged Higgs $H^\pm$.

Our conclusions are that the largest Higgs masses are realized on the focal surface of the hyperbolic branch of radiative electroweak symmetry breaking. We also point out that low values of $\mu \sim 150$ GeV are consistent with heavy squarks and sleptons in the 10 TeV region or larger. We find that $m_{h^0} \in (123\text{--}127)$ GeV does allow for light third-generation stop as low as $m_{\tilde{t}_1} > 230$ GeV, though the second-generation squarks are at least $m_{\tilde{q}} > 1.5$ TeV and second-generation sleptons are at least 475 GeV. Thus, the restriction of the light Higgs boson to the mass window $m_{h^0} \in (123\text{--}127)$ GeV provides further constraints on the sparticle spectrum that are complementary to the direct searches for sparticles at the LHC.

Further, we find precise predictions for dark matter if the light Higgs boson mass lies between 123 GeV and 127 GeV. For these light Higgs boson masses, the corresponding range of the lightest neutralino mass would be accessible in the next generation of direct detection dark matter experiments. The light Higgs boson in the 123 GeV and 127 GeV range was shown to be generic for the case of heavy scalars in minimal supergravity with $|A_0/m_0| \sim \mathcal{O}(1)$.

[1] P. W. Higgs, Phys. Lett. **12**, 132 (1964); Phys. Rev. Lett. **13**, 508 (1964); G. S. Guralnik, C. R. Hagen, and T. W. B. Kibble, Phys. Rev. Lett. **13**, 585 (1964); F. Englert and R. Brout, Phys. Rev. Lett. **13**, 321 (1964); P. W. Higgs, Phys. Rev. **145**, 1156 (1966).

[2] F. Gianotti (ATLAS), "Update on the Standard Model Higgs searches in ATLAS," in Joint CMS/ATLAS Seminar at CERN, December 13, 2011 (unpublished); G. Tonelli (CMS), "Update on the Standard Model Higgs searches in ATLAS," in Joint CMS/ATLAS Seminar at CERN, December 13, 2011 (unpublished).

[3] A. H. Chamseddine, R. L. Arnowitt, and P. Nath, Phys. Rev. Lett. **49**, 970 (1982); P. Nath, R. L. Arnowitt, and A. H. Chamseddine, Phys. Lett. B **121**, 33 (1983).

[4] P. Nath, arXiv:0307123.

[5] L. E. Ibanez and G. G. Ross, C.R. Physique **8**, 1013 (2007).

[6] P. Nath, B. D. Nelson, H. Davoudiasl, B. Dutta, D. Feldman, Z. Liu, T. Han, P. Langacker *et al.*, Nucl. Phys. B, Proc. Suppl. **200-202**, 185 (2010).

[7] D. Feldman, Z. Liu, and P. Nath, Phys. Lett. B **662**, 190 (2008).

[8] D. Feldman, Z. Liu, and P. Nath, Phys. Rev. D **81**, 095009 (2010).

[9] D. Feldman, G. Kane, R. Lu, and B. D. Nelson, Phys. Lett. B **687**, 363 (2010).

[10] H. Baer, V. Barger, A. Lessa, and X. Tata, J. High Energy Phys. 06 (2010) 102.

[11] B. Altunkaynak, M. Holmes, P. Nath, B. D. Nelson, and G. Peim, Phys. Rev. D **82**, 115001 (2010).

[12] CMS Collaboration, Phys. Lett. B **698**, 196 (2011); CMS Collaboration, Phys. Rev. Lett. **107**, 221804 (2011); CMS CollaborationReport No. CMS-PAS-SUS-11-005; CMS CollaborationReport No. CMS-PAS-SUS-11-006; CMS CollaborationReport No. CMS-PAS-SUS-11-013; CMS CollaborationReport No. CMS-PAS-SUS-11-015.

[13] ATLAS Collaboration, Phys. Rev. Lett. **106**, 131802 (2011).

[14] ATLAS Collaboration, Phys. Lett. B **701**, 186 (2011).

[15] ATLAS Collaboration, Report No. ATLAS-CONF-2011-086.

[16] G. Aad *et al.* (ATLAS Collaboration), arXiv:1109.6572; , J. High Energy Phys. 11 (2011) 099.

[17] D. Feldman *et al.*, Phys. Rev. D **84**, 015007 (2011); B.C. Allanach, Phys. Rev. D **83**, 095019 (2011); S. Scopel *et al.*, Phys. Rev. D **83**, 095016 (2011); O. Buchmueller *et al.*, Eur. Phys. J. C **71**, 1634 (2011); M. Guchait and D. Sengupta, Phys. Rev. D **84**, 055010 (2011); P. Bechtle *et al.*, Phys. Rev. D **84**, 011701 (2011); D.S.M. Alves *et al.*, J. High Energy Phys. 10 (2011) 012; B.C. Allanach *et al.*, J. High Energy Phys. 06 (2011) 035; J.A. Conley *et al.*, arXiv:1103.1697; T. Li *et al.*, arXiv:1103.2362; Phys. Rev. D **84**, 076003 (2011); J. Kozaczuk and S. Profumo, J. Cosmol. Astropart. Phys. 11 (2011) 031; M.A. Ajaib *et al.*, Phys. Lett. B **705**, 87 (2011); O. Buchmueller *et al.*, arXiv:1110.3568; A. Arbey *et al.*, Eur. Phys. J. C **72**, 1847 (2012); X.J. Bi *et al.*, arXiv:1111.2250; N. Desai and B. Mukhopadhyaya, arXiv:1111.2830; M.A. Ajaib, T. Li, and Q. Shafi, arXiv:1111.4467.

[18] S. Akula, N. Chen, D. Feldman, M. Liu, Z. Liu, P. Nath, and G. Peim, Phys. Lett. B **699**, 377 (2011).

[19] S. Akula, D. Feldman, Z. Liu, P. Nath, and G. Peim, Mod. Phys. Lett. A **26**, 1521 (2011).

[20] S. Akula, D. Feldman, P. Nath, and G. Peim, Phys. Rev. D **84**, 115011 (2011).

[21] S. Profumo, Phys. Rev. D **84**, 015008 (2011); O. Buchmueller *et al.*, Eur. Phys. J. C **71**, 1722 (2011); G. Bertone *et al.*, J. Cosmol. Astropart. Phys. 01 (2012) 015; A. Fowlie, A. Kalinowski, M. Kazana, L. Roszkowski, and Y.L.S. Tsai, arXiv:1111.6098.

[22] D. Grellscheid *et al.*, arXiv:1111.3365.

[23] U. Ellwanger *et al.*, J. High Energy Phys. 09 (2011) 105.

[24] L.J. Hall, J.D. Lykken, and S. Weinberg, Phys. Rev. D **27**, 2359 (1983).

[25] P. Nath and R.L. Arnowitt, and A.H. Chamseddine, Nucl. Phys. **B227**, 121 (1983).

[26] R.L. Arnowitt and P. Nath, Phys. Rev. Lett. **69**, 725 (1992); Phys. Lett. B **287**, 89 (1992).

[27] Y. Okada, M. Yamaguchi, and T. Yanagida, Prog. Theor. Phys. **85**, 1 (1991); J.R. Ellis, G. Ridolfi, and F. Zwirner, Phys. Lett. B **257**, 83 (1991); H.E. Haber and R. Hempfling, Phys. Rev. Lett. **66**, 1815 (1991); H.E. Haber, R. Hempfling, and A.H. Hoang, Z. Phys. C **75**, 539 (1997).

[28] G.L. Kane, C.F. Kolda, and J.D. Wells, Phys. Rev. Lett. **70**, 2686 (1993); J.R. Espinosa and M. Quiros, Phys. Lett. B **302**, 51 (1993).

[29] J.A. Casas, J.R. Espinosa, M. Quiros, and A. Riotto, Nucl. Phys. **B436**, 3 (1995).

[30] M.S. Carena, M. Quiros, and C.E.M. Wagner, Nucl. Phys. **B461**, 407 (1996); Phys. Lett. B **355**, 209 (1995).

[31] J.R. Espinosa and R. -J. Zhang, Nucl. Phys. **B586**, 3 (2000).

[32] M.S. Carena, P.H. Chankowski, S. Pokorski, and C.E.M. Wagner, Phys. Lett. B **441**, 205 (1998) and references therein.

[33] A. Djouadi, Phys. Rep. **459**, 1 (2008).

[34] B.C. Allanach, A. Djouadi, J.L. Kneur, W. Porod, and P. Slavich, J. High Energy Phys. 09 (2004) 044.

[35] K.L. Chan, U. Chattopadhyay, and P. Nath, Phys. Rev. D **58**, 096004 (1998); U. Chattopadhyay, A. Corsetti, and P. Nath, Phys. Rev. D **68**, 035005 (2003).

[36] D. Feldman, G. Kane, E. Kuflik, and R. Lu, Phys. Lett. B **704**, 56 (2011).

[37] H. Baer, V. Barger, P. Huang, and A. Mustafayev, Phys. Rev. D **84**, 091701 (2011); I. Gogoladze, Q. Shafi, and C.S. Un., arXiv:1112.2206.

[38] K. Tobe and J.D. Wells, Phys. Rev. D **66**, 013010 (2002).

[39] N. Arkani-Hamed, S. Dimopoulos, G.F. Giudice, and A. Romanino, Nucl. Phys. **B709**, 3 (2005).

[40] B. Kors and P. Nath, Nucl. Phys. **B711**, 112 (2005).

[41] M.E. Cabrera, J.A. Casas, and A. Delgado, Phys. Rev. Lett. **108**, 021802 (2012).

[42] G.F. Giudice and A. Strumia, Nucl. Phys. **B858**, 63 (2012).

[43] K.S. Babu, I. Gogoladze, M.U. Rehman, and Q. Shafi, Phys. Rev. D **78**, 055017 (2008); S.P. Martin, Phys. Rev. D **81**, 035004 (2010).

[44] K. Nakamura *et al.* (Particle Data Group Collaboration), J. Phys. G **37**, 075021 (2010).

[45] E. Komatsu *et al.*, Astrophys. J. Suppl. Ser. **192**, 18 (2011).

[46] D. Feldman, Z. Liu, P. Nath, and G. Peim, Phys. Rev. D **81**, 095017 (2010); D. Feldman, P. Fileviez Perez, and P. Nath, J. High Energy Phys. 01 (2012) 038.

[47] A. Djouadi, M. Drees, and J.L. Kneur, J. High Energy Phys. 03 (2006) 033.

[48] E. Barberio *et al.*, arXiv:0808.1297.

[49] CDF Collaboration, Phys. Rev. Lett. **107**, 191801 (2011); CMS and LHCb Collaborations, Report Nos. LHCb-CONF-2011-047 and CMS PAS BPH-11-019.

[50] V.M. Abazov *et al.* (D0 Collaboration), Phys. Lett. B **693** (2010) 539.

[51] M. Misiak *et al.*, Phys. Rev. Lett. **98**, 022002 (2007).

[52] S. Akula, M. Liu, P. Nath, and G. Peim, Phys. Lett. B **709**, 192 (2012).

[53] G. Belanger *et al.*, Comput. Phys. Commun. **180**, 747 (2009); **182**, 842 (2011).

[54] B.C. Allanach, Comput. Phys. Commun. **143**, 305 (2002). Version 3.2.4 was used in this analysis.

[55] D. Feldman *et al.*, J. High Energy Phys. 04 (2008) 054; Phys. Lett. B **662**, 190 (2008); Phys. Rev. Lett. **99**, 251802 (2007); C.F. Berger *et al.*, J. High Energy Phys. 02 (2009) 023; B. Altunkaynak *et al.*, Eur. Phys. J. Plus **127**, 2 (2012).

[56] P. Nath and R.L. Arnowitt, Phys. Rev. D **56**, 2820 (1997).

[57] H. Baer, C. Balazs, A. Belyaev, T. Krupovnickas, and X. Tata, J. High Energy Phys. 06 (2003) 054.

[58] J. L. Feng, K. T. Matchev, and T. Moroi, Phys. Rev. Lett. **84**, 2322 (2000); Phys. Rev. D **61**, 075005 (2000); J. L. Feng, K. T. Matchev, and D. Sanford, arXiv:1112.3021.

[59] U. Chattopadhyay, T. Ibrahim, and P. Nath, Phys. Rev. D **60**, 063505 (1999).

[60] J. R. Ellis, A. Ferstl, and K. A. Olive, Phys. Lett. B **481**, 304 (2000).

[61] E. Aprile *et al.* (The XENON100 Collaboration), Phys. Rev. Lett. **107**, 131302 (2011); , Phys. Rev. Lett. **105**, 131302 (2010); , Phys. Rev. D **84**, 052003 (2011).

[62] E. Aprile (The XENON100 Collaboration), ''The XENON Dark Matter Search,'' in WONDER Workshop: LNGS March 22-23, 2010 (unpublished).

[63] B. Cabrera (SuperCDMS Collaboration), ''SuperCDMS Development Project,'' 2005, http://www.fnal.gov/directorate/program_planning/April2005PACPublic/Cabrera_April2005PAC.pdf.

[64] H. Baer, V. Barger, and A. Mustafayev, arXiv:1112.3017; A. Arbey, M. Battaglia, A. Djouadi, F. Mahmoudi, and J. Quevillon, Phys. Lett. B **708**, 162 (2012).